ACS APPLIED MATERIALS & INTERFACES

www.acsami.org Research Article

Wearable Pressure Sensors Based on MXene/Tissue Papers for Wireless Human Health Monitoring

Li Yang,* Hongli Wang, Wenjing Yuan, Yuhang Li, Peng Gao, Naveen Tiwari, Xue Chen, Zihan Wang, Guangyu Niu, and Huanyu Cheng*

Cite This: *ACS Appl. Mater. Interfaces* 2021, 13, 60531−60543 Read Online

ACCESS | Metrics & More | Article Recommendations | SI Supporting Information

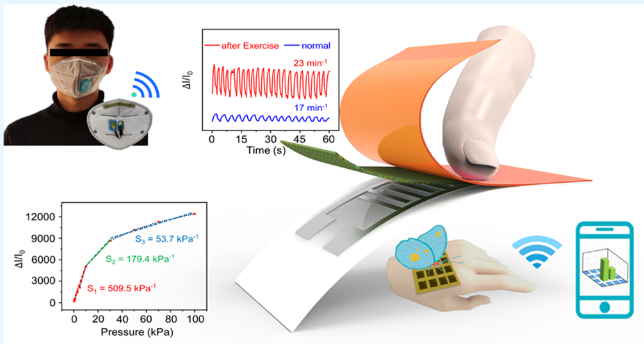
[redacted]

ABSTRACT: Though the widely available, low-cost, and disposable papers have been explored in flexible paper-based pressure sensors, it is still difficult for them to simultaneously achieve ultrahigh sensitivity, low limit and broad range of detection, and high-pressure resolution. Herein, we demonstrate a novel flexible paper-based pressure sensing platform that features the MXene-coated tissue paper (MTP) sandwiched between a polyimide encapsulation layer and a printing paper with interdigital electrodes. After replacing the polyimide with weighing paper in the MTP pressure sensor, the silver interdigital electrodes can be recycled through incineration. The resulting pressure sensor with polyimide or paper encapsulation exhibits a high sensitivity of 509.5 or 344.0 kPa^{-1}, a low limit (~1 Pa) and a broad range (100 kPa) of detection, and outstanding stability over 10 000 loading/unloading cycles. With ultrahigh sensitivity over a wide pressure range, the flexible pressure sensor can monitor various physiological signals and human movements. Configuring the pressure sensors into an array layout results in a smart artificial electronic skin to recognize the spatial pressure distribution. The flexible pressure sensor can also be integrated with signal processing and wireless communication modules on a face mask as a remote respiration monitoring system to wirelessly detect various respiration conditions and respiratory abnormalities for early self-identification of opioid overdose, pulmonary fibrosis, and other cardiopulmonary diseases.

KEYWORDS: *piezoresistive pressure sensor, MXene, paper-based electronic devices, wearable electronics, wireless healthcare monitoring, electronic skins*

1. INTRODUCTION

Soft deformable pressure sensors provide unique application opportunities in electronic skins,[1,2] human−machine interfaces,[3] biomedical monitoring,[4−6] breath analysis,[7,8] and intelligent robotics.[9,10] Compared to those based on capacitive,[11,12] piezoelectric,[13−15] or triboelectric effects,[16,17] piezoresistive pressure sensors[18,19] are associated with high sensitivity, cost-efficient fabrication, and simple signal detection.[20,21] However, the high sensitivity in most flexible piezoresistive pressure sensors often relies on complicated 3D structures from costly and complex fabrication processes (spin-coating, photolithography, vacuum deposition, and dry/wet etching). In addition, most of the key components in the sensors are not disposable or biodegradable, posing environmental concerns.

In contrast to the flexible pressure sensors based on polyimide (PI),[22] polydimethylsiloxane,[23,24] polyester,[25] or poly(ethylene terephthalate),[26] the low-cost paper-based pressure sensors[27−30] can be disposable and environmentally friendly. Though delicate microstructures (e.g., micropyramids,[31,32] microdomes,[33−35] air bubbles in the elastomeric foams[36]) prepared by lithography or templated methods can improve the pressure sensing performance, the complicated processes and expensive equipment are challenging for mass production. As a simple alternative, paper with a porous cellulose microstructure starts to gain popularity in creating highly sensitive pressure sensors. Though various conductive nanomaterials (e.g., metal nanoparticles/nanowires,[37−39] carbon nanotubes,[40] graphene,[41,42] and their nanocomposites[6]) have been explored, the resulting paper-based piezoresistive pressure sensors do not provide a sufficient sensing performance. It is still highly desirable to demonstrate the paper-based piezoresistive pressure sensors with ultrahigh sensitivity, low limit and broad range of detection, fast response/recovery, and excellent stability.

Received: November 12, 2021
Accepted: November 30, 2021
Published: December 13, 2021

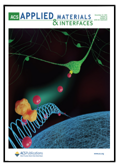

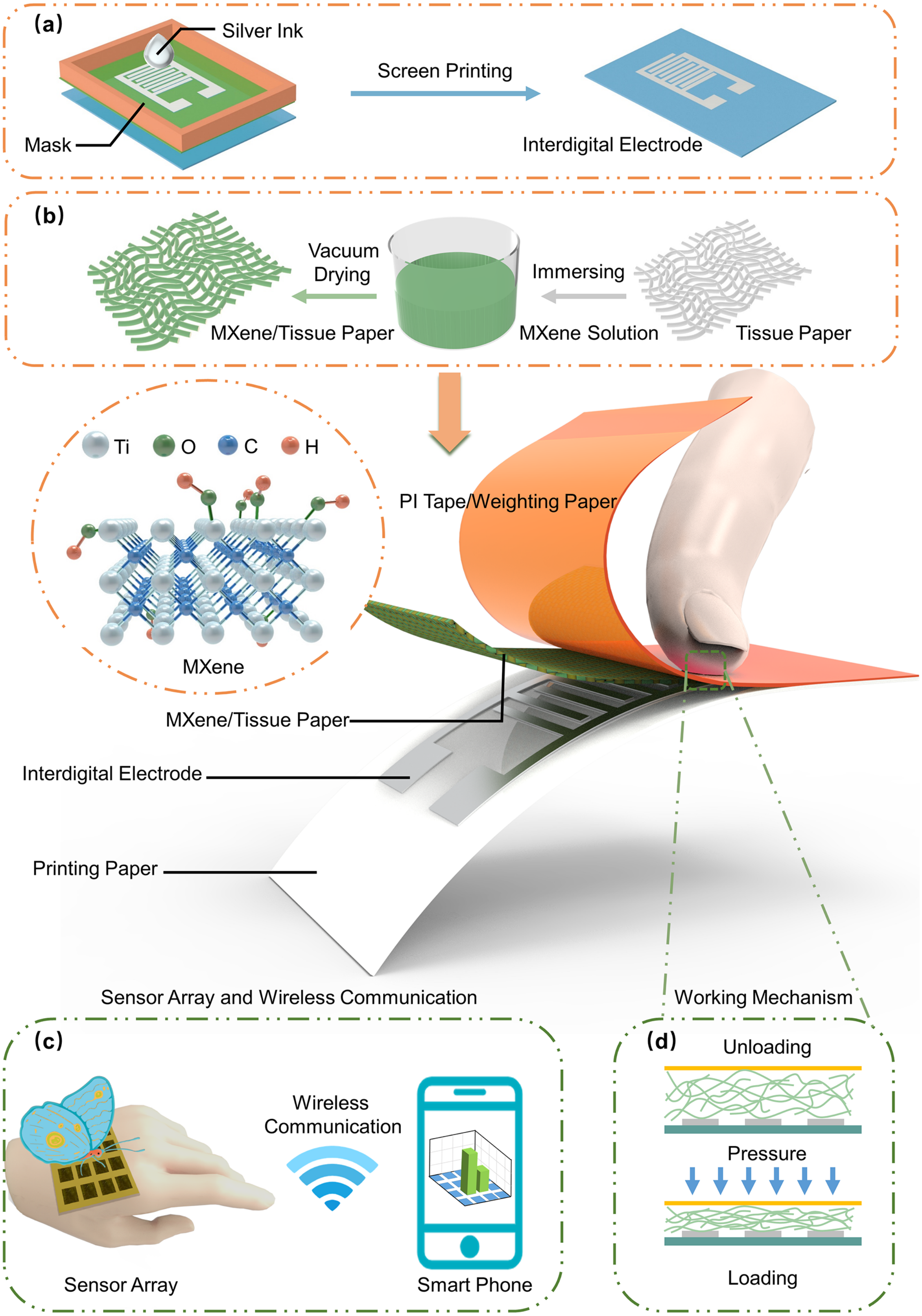

Figure 1. Schematic to show the preparation processes of the paper-based wireless wearable pressure sensor consisting of (a) the interdigital electrodes and (b) MXene/tissue paper, which can be configured in (c) an array layout to wirelessly detect the spatial pressure distribution, with the working mechanism shown in (d).

https://doi.org/10.1021/acsami.1c22001
ACS Appl. Mater. Interfaces 2021, 13, 60531−60543

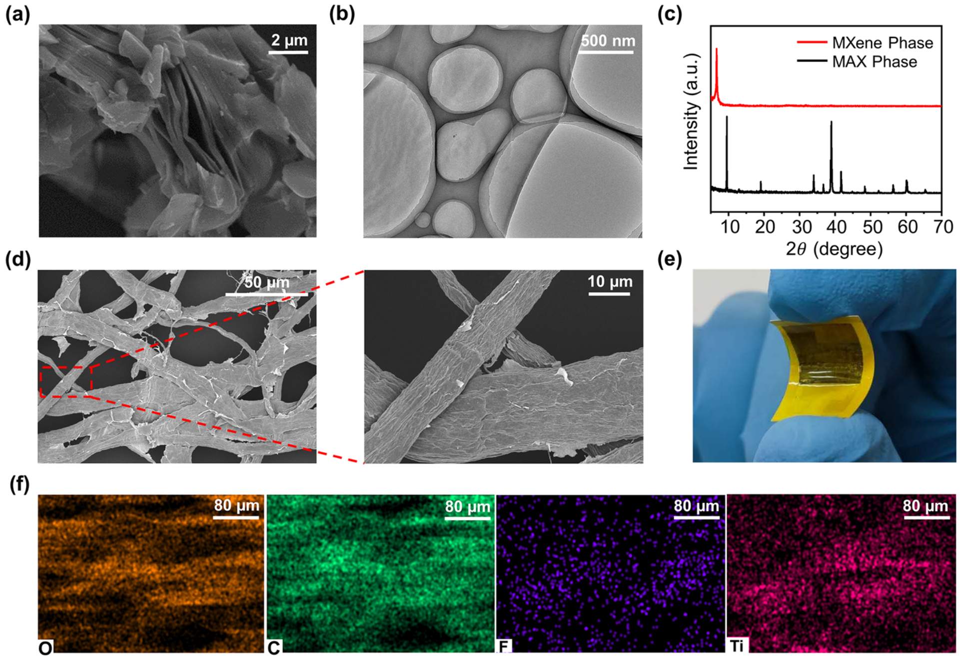

Figure 2. Characterization of the flexible MTP pressure sensor. (a) SEM image of the MXene powder. (b) TEM image of the MXene nanosheets. (c) XRD spectra of MXene and MAX (Ti_3AlC_2). (d) SEM images of the tissue paper after the MXene coating with the zoom-in to show the fiber structure of the MTP. (e) Photograph of the flexible MTP pressure sensor bent upon compressive force. (f) Elemental mapping of the MXene/tissue paper for C, O, F, and Ti.

As an emerging 2D material with excellent conductivity and high specific surface, MXene has been explored on flexible substrates (e.g., polymer, fabric, protein composites) for piezoresistive pressure sensors.[43−46] However, the disposable pressure sensing platform that combines paper with MXene for ultrahigh sensitivity over a wide detection range from cost-effective fabrication is still not available. Herein, we design and demonstrate a flexible paper-based pressure sensing platform that features the MXene-coated tissue paper (MTP) sandwiched between an encapsulation layer (PI film or weighing paper) and a printing paper with interdigital electrodes. Because of the highly porous 3D structure of the MTP and high specific surface area of MXene, the MTP pressure sensor encapsulated by the 35 μm-thick PI film exhibits an ultrahigh sensitivity of 509.5 kPa^{-1}, a low limit (1 Pa) and a broad range (100 kPa) of detection, and excellent stability over 10 000 loading/unloading cycles. More importantly, replacing the PI film with the weighing paper further results in a recyclable paper-based MTP pressure sensor with a sensitivity of 344.0 kPa^{-1} over the same sensing range of up to 100 kPa. The paper-based pressure sensor can be disposed of by incineration (<20 s) to recycle the silver electrodes for reuse. With ultrahigh sensitivity over a broad pressure range, the MTP pressure sensor has then been explored to accurately detect varying physiological signals and human motions. The integrated respiration monitoring system with signal processing and wireless communication modules is capable of wirelessly detecting respiration rate, respiratory depth, and respiratory arrest for early self-identification of opioid overdose. The detected respiratory abnormalities can also be applied for pulmonary fibrosis and other cardiopulmonary diseases.

2. RESULTS AND DISCUSSION

2.1. Preparation and Working Mechanism of the MTP Paper-Based Pressure Sensor. The paper-based wireless wearable pressure sensor features a sandwich device structure with MXene/tissue paper sandwiched between an encapsulation layer and a printing paper substrate with printed silver interdigitated electrodes (Figure 1 and cross-section view shown in Figure S1). In brief, the interdigitated electrodes with a finger width of 0.8 mm and spacing of 0.6 mm (Figure S2) in an area of 14.7 mm × 10 mm were fabricated on a printing paper by screen-printing silver paste (Figure 1a). Next, a sheet of tissue paper (10 × 10 mm^2) immersed in the MXene dispersion and dried in a vacuum prepared the MXene-coated tissue paper (Figure 1b) in a black color (Figure S3). After placing the MXene/tissue paper at the center of interdigitated electrodes, using an adhesive polyimide PI tape or weighing paper to encapsulate the entire structure yields a flexible MXene/tissue paper (MTP) pressure sensor. As a representative example, we first systematically investigated the pressure sensing performance of the MTP sensor encapsulated by a 35 μm-thick PI film. The MTP pressure sensor can be arranged into an array layout and integrated with a wireless transmitter as intelligent artificial electronic skins for spatial pressure mapping and human-interactive sensing (Figure 1c).

The simple resistance-based sensing of the MTP pressure sensor relies on the pressure-induced resistance change (Figure 1d). It is highly desirable to directly measure the cross-section morphology of the sensor under different pressures in the experiment to support the mechanism analysis.[25] The total resistance is the sum of the electrode, the MTP, and the MTP/electrode contact resistances (Figure S4). When the applied pressure increases, the MXene nanosheets move closer to increase the conductive pathway as the interstice of the MXene/tissue paper is compressed. The contact areas between the MTP and the interdigitated electrodes are also increased for reduced contact resistance upon further increased pressure. As a result, the MTP pressure sensor exhibits the salient feature of ultrahigh sensitivity over a wide detection range.

https://doi.org/10.1021/acsami.1c22001
ACS Appl. Mater. Interfaces 2021, 13, 60531−60543

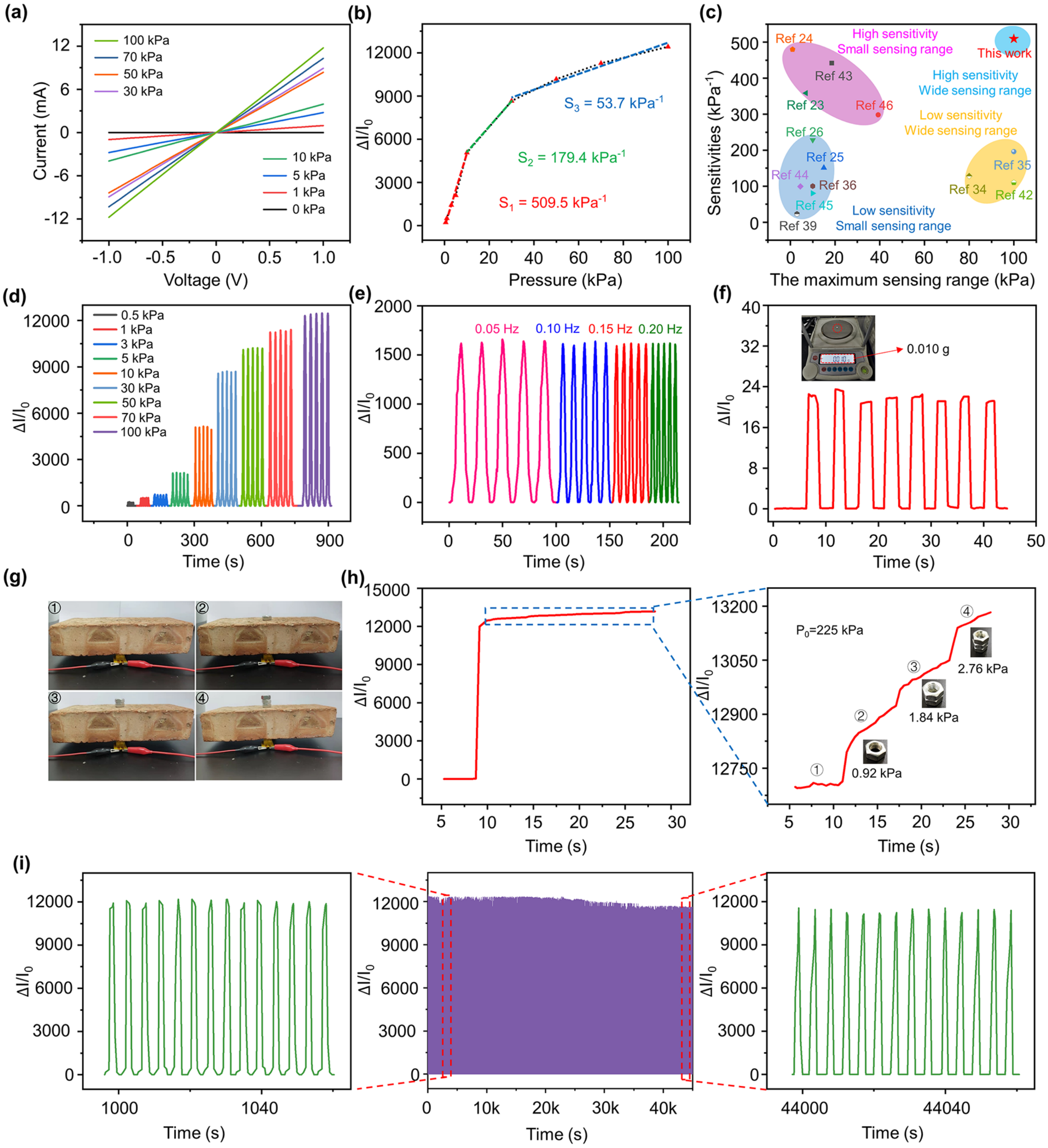

Figure 3. Electromechanical properties of the flexible MTP pressure sensor. (a) *I*−*V* curves for varying pressure loading values. (b) Relative current change of the MTP pressure sensor under different external pressures, from which (c) the sensitivity of our MTP pressure sensor is obtained and compared with previous literature reports. Relative current response of the MTP pressure sensor under cyclic loading/unloading with (d) the pressure from 0.5 to 100 kPa and (e) the frequency from 0.05 to 0.20 Hz for 4 kPa. (f) Current response to 1 Pa for eight cycles. (g) Photographs of the MTP pressure sensor with a brick and varying numbers of nuts placed on top. (h) Detection of small pressure increments (0.92, 1.84, and 2.76 kPa) under high pressure with nuts placed on a brick weighing 225 kPa. (i) Repeatability test of the MTP sensor over 10 000 loading/unloading cycles (100 kPa).

2.2. Material Characterization of the Paper-Based MTP Pressure Sensor. The material and chemical properties of the flexible MTP pressure sensors were first characterized (Figure 2). The scanning electron microscope (SEM) image shows an accordion-like layered structure in the $Ti_3C_2T_x$ powders (Figure 2a). In the transmission electron microscope (TEM) image, the MXene nanosheets show a slightly wrinkled morphology with a lateral dimension of hundred nanometers to micrometers (Figure 2b). The thickness also indicates single-layer to few-layered MXene. Figure 2c shows the (002) peak shift from 9.5° in the MAX phase to 6.6° in MXene by the X-ray diffraction (XRD) patterns, which indicates the successful production of MXene. The X-ray photoelectron spectroscopy (XPS) measurements of the MXene further confirm the existence of Ti, C, O, and F (Figure S5a). In particular, Figure S5b displays the Ti 2p spectrum fitted with three doublets (Ti $2p_{3/2}$−Ti $2p_{1/2}$). The Ti $2p_{3/2}$ components at 455.3, 456.2, and 458.4 eV are from Ti—C, Ti (II), and

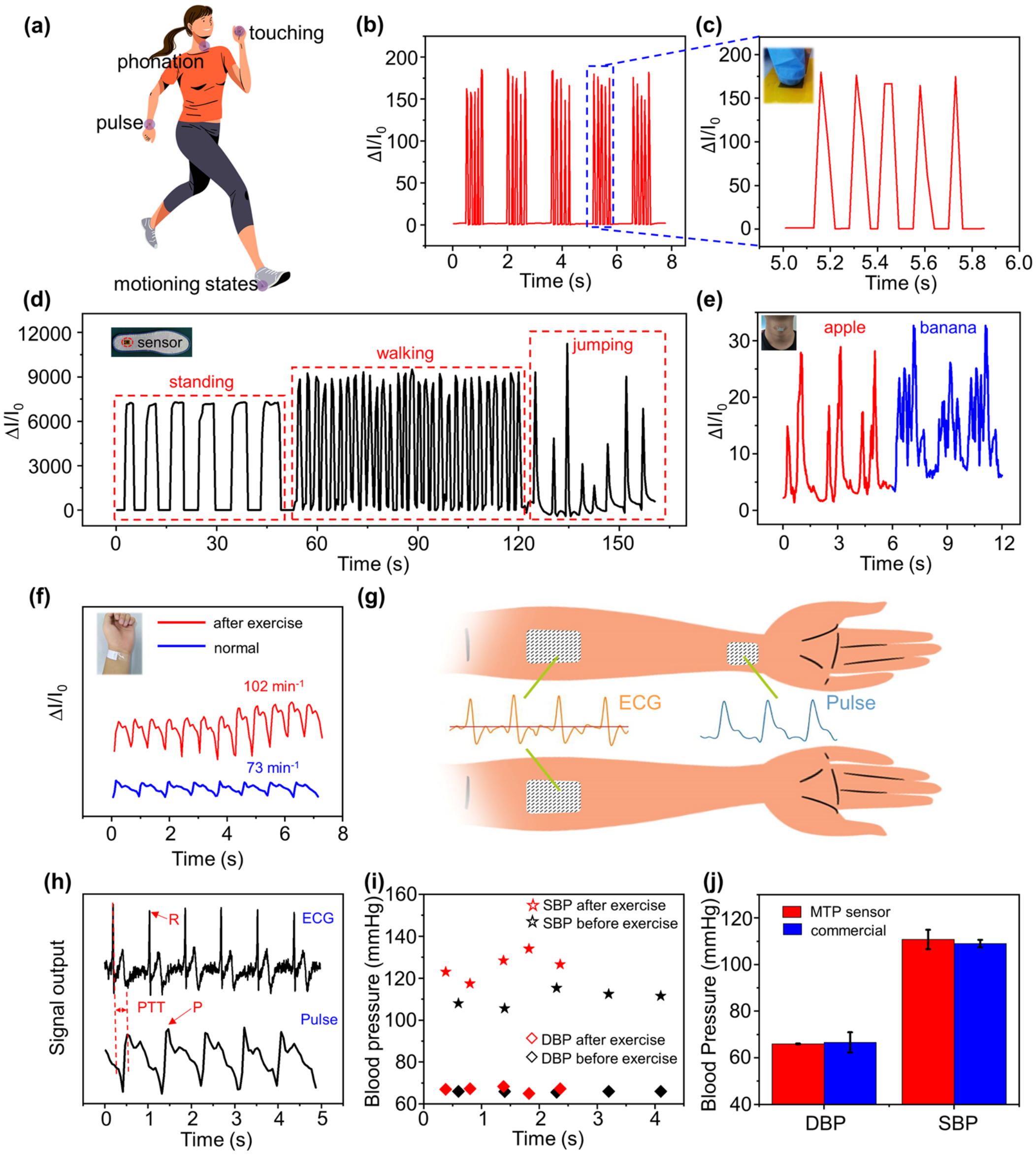

Figure 4. Applications of the MTP pressure sensor to monitor human physiological signals. (a) Schematic to show the various scenarios of physiological monitoring. (b) Relative current change of the sensor under a static frequency of 5 Hz to simulate the tremor in early stage Parkinson's disease, with a zoom-in view shown in (c) and a photograph of the imitated knocking in the inset. Relative current variation of the sensor caused by (d) three different motion states with the pressure sensor on top of the insole (i.e., standing, walking, and jumping) and by (e) throat movement during reading the words of "apple" and "banana". Inset images show the MTP pressure sensor placed on the heel of the insole or attached to the tester's neck, respectively. (f) Wrist pulse signal of the human before and after exercise, with the sensor attached to a wrist shown in the inset. (g) Schematic illustration to show the sensors placement and (h) the concurrent recording of ECG and arterial pulse signals with the pulse transit time (PTT) indicated for blood pressure monitoring. (i) Calculated beat-to-beat systolic blood pressures (SBPs, stars) and diastolic blood pressures (DBPs, rhombus) before (black) and after (red) exercise on the basis of the PTT method. (j) Comparisons of the DBPs and SBPs measured using the PTT method with those measured by a commercial sphygmomanometer.

Ti—O bonds, respectively. The C 1s level is fitted with five types of carbon atoms (Figure S5c), with 281.8, 282.1, 284.8, 286.6, and 288.2 eV for C—Ti, Ti—C—O, C—C, C—O, and O—C═O, respectively.

The SEM images of the tissue paper before (Figure S6a,b) and after (Figure 2d) MXene coating indicate uniform coating onto cellulose fibers in the tissue paper with a well-preserved porous structure. The main elements (e.g., Ti, C) and surface terminations (e.g., O, F) of MXene in the elemental mapping further confirm the uniform distribution of the surface-functionalized MXene on the tissue paper (Figure 2f).

Because the unique 2D structure of the MXene sheets provides a good conductive pathway, the sheet resistance of the MTP gradually decreases from 5 MΩ/□ to 2.5 kΩ/□ as the concentration of the MXene dispersion increases from 0.5 to 1.0 mg/mL (Figure S7). The sheet resistance also affects the sensitivity of the MTP pressure sensors with a sensitivity peak obtained at 23.4 kΩ/□ in the investigated range (Figure S8). Furthermore, benefiting from the thin geometry, the MTP pressure sensor exhibits excellent flexibility upon compressive forces (Figure 2e).

2.3. Sensing Properties of the MTP Pressure Sensor.

The performance of the MTP pressure sensor depends on the design parameters, including the thickness of the encapsulation layer and layers of the tissue paper (Figure S9). The current responses (defined as the ratio of the current change to its initial value before pressure loading) of the pressure sensor in the range from 0.5 to 100 kPa sharply decrease as the thickness of the PI encapsulation layer increases from 35 to 50 and then to 60 μm. The results can be understood as the bending stiffness of a thin film scales with the cubic of its thickness.[47] The number of MXene/tissue layers also affects the sensing performance, as revealed in the results of sensors with 1, 2, or 3 layers of MXene/tissue paper (Figure S9b). The sensitivity defined as $S = \delta\ (\Delta I/I_0)/\delta P$ in the small pressure range (0.5−10 kPa) slightly enhances from 509.5 to 545.3 and then to 650.7 (Figure S9c) but decreases in the large pressure range (10−100 kPa). The slight enhancement in the small pressure range is attributed to the pressure-reduced air gaps between layers for increased resistance change and higher sensitivity.[27] Meanwhile, the multilayered MXene/tissue structure forms a parallel connection for a lower initial resistance and a larger initial current than that of the single-layer MTP pressure sensor, resulting in a smaller current change. For a pressure of 100 kPa, the current variation ratio decreases from 12×10^3 for the single-layer MTP sensor to 7.8×10^3 for that of the three-layer one. As a result of the above considerations, the single-layer MTP sensor with a 35 μm-thick encapsulation is investigated in the following study for the balanced flexibility, sensitivity, and working range, unless specified otherwise. The measurement of the current−voltage (I−V) curves of the MTP pressure sensor at varying pressure values provides the characterization of its electromechanical properties. The I−V curves as a function of the pressure ranging from 0 to 100 kPa show excellent linear characteristics (Figure 3a), indicating stable response and capability to distinguish the pressure over a wide range. As the pressure increases from 0.5 to 100 kPa, the current response increases in a piecewise linear manner (Figure 3b). The sensitivities (slopes in Figure 3b) of the MTP sensor are obtained as 509.5, 179.4, and 53.7 kPa^{-1} in the pressure ranges 0.5−10, 10−30, and 30−100 kPa, respectively. Because of the highly porous 3D structure, our MTP pressure sensor with an ultrahigh sensitivity over a broad pressure range compares favorably with the state-of-the-art flexible piezoresistive pressure sensors (Figure 3c and Table S1). In particular, the ultrahigh sensitivity of 509.5 kPa^{-1} in the pressure range of 0.5−10 kPa is important to detect human physiological signals (e.g., pulse profile and respiration).[48] The dynamic pressure-sensitive response curves in the pressure range from 500 Pa to 100 kPa (Figure 3d) and frequencies from 0.05 to 0.2 Hz for a 4 kPa pressure (Figure 3e) demonstrate outstanding stability over wide pressure and frequency ranges. The standard deviation measured from five randomly selected pressure sensors in the pressure range from 0.5 to 100 kPa is only 2% (Figure S10), showcasing high reproducibility. Besides the large pressure, the MTP pressure sensor could also detect subtle pressures of 1 Pa (Figure 3f and Movie S1), indicating a limit of detection (LOD) of <1 Pa. Besides ultrahigh sensitivity over a broad detection range and a low LOD, the high sensitivity under high pressure also allows the MTP sensor to detect pressures at a high resolution. An aluminum block of $10 \times 10 \times 10\ \text{mm}^3$ placed under a brick of ∼2.25 kg provides a reference pressure of $P_0 = 225$ kPa. Next, gently placing one, two, and three nuts on top of the brick leads to an effective pressure increment ΔP of 0.92, 1.84, and 2.76 kPa, respectively (Figure 3g). The corresponding relative current changes confirm the precise recording and differentiation of these pressure increments (Figure 3h). Therefore, our MTP pressure sensor is demonstrated to identify the tiny changes in pressure under both low and extremely high pressures. Additionally, the performance of the MTP pressure sensor is highly stable and reliable with nearly invariant relative current changes even over 10 000 loading/unloading cycles under different pressure values of 10, 30, and 100 kPa (Figure 3i and Figure S11). The MTP pressure sensor also exhibits rapid response/recovery rates (150/60 ms) (Figure S12), enabling the detection of human physiological signals in real time. In addition to pressure, the MTP sensor can also detect bending deformations (Figure S13), as the relative current gradually increases with the increasing bending strain.

2.4. Applications in Human Physiological Activity Measurements. The flexible MTP pressure sensor with an ultrahigh sensitivity over a broad pressure range and fast response/recovery can be applied to capture varying human physiological signals (Figure 4a). The MTP pressure sensor is capable of capturing low-frequency changes such as static tremors (simulated by knocking; frequency of 4−6 Hz) in early stage Parkinson's disease for potential disease diagnosis (Figure 4b,c). The capability of our device to detect the pressure from a wide range is demonstrated by monitoring the plantar pressure of an adult male (70 kg, 10 U.S. size for the shoe) with the sensor on the bottom heel region of the insole (Figure 4d). The MTP pressure sensor placed on the top of the insole gives a higher relative current change compared with those placed below the insole (Figure S14) due to a much larger initial current from the weight of the insole. The three different motion states from standing, walking, and jumping can be clearly distinguished from the signal magnitude created by the progressively increasing pressure (Figure 4d). Meanwhile, the signal from standing is relatively periodic, whereas that from high-intensity jumping exhibits sharp peaks from the impact of landing. By combining the spatiotemporal signal captured by the MTP pressure sensor on the human throat, the tiny vibrations produced by phonation can be potentially used for phonation rehabilitation training and voice recognition. In the proof-of-concept demonstration, the words "apple" and "banana" can be differentiated (Figure 4e).

As one important vital sign, pulse rate monitoring from the MTP pressure sensor on the wrist shows high potential for the diagnosis and prevention of cardiovascular disease.[49] The recorded real-time wrist pulse signal with clearly identified characteristic peaks (i.e., percussion, tidal, and diastolic waves) from a healthy human subject (24 years old, male) shows an increased rate from 73 to 102 min^{-1} after exercise (Figure 4f). The comparison in the extracted single-pulse waveforms before (Figure S15a) and after exercise (Figure S15b) also shows increased intensity and disappearance of the T wave after exercise.

The concurrent recording of the arterial pulse with electrocardiograph (ECG) signals can provide real-time cuffless blood pressure measurements such as systolic and diastolic blood pressures (SBPs/DBPs) for diagnosis and prophylaxis of cardiovascular diseases. Due to the excellent conductivity of MXene/tissue paper, it can be used as electrodes for ECG measurement (Figure S16), with comparable signal quality as that from the commercial Ag/AgCl electrodes (Figure S17). Moreover, the signal-to-noise ratio (SNR) of the ECG signals at rest can be calculated from[50]

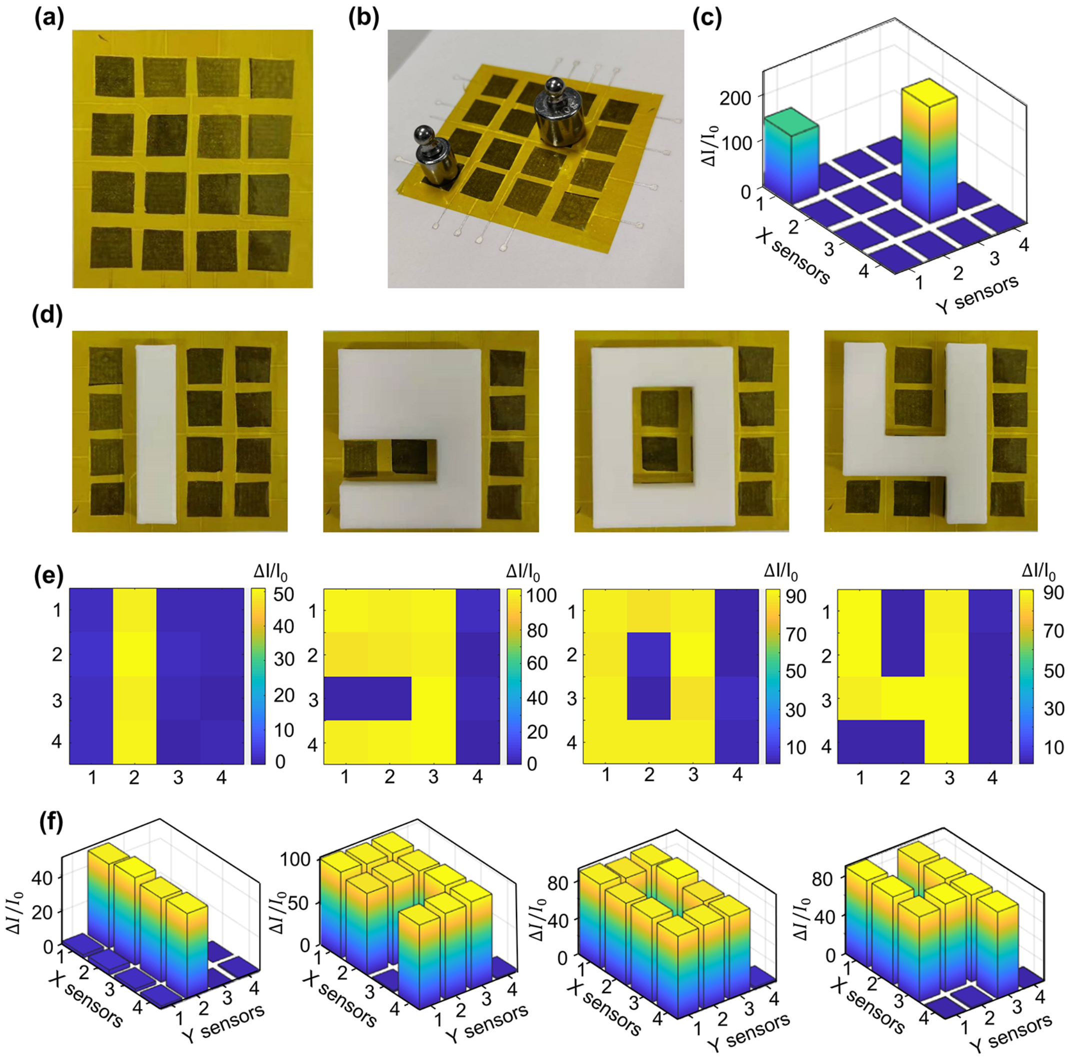

Figure 5. Demonstration of the MTP pressure sensor array to monitor spatial pressure distribution. Images of (a) the sensor array with (b) two different weights placed on the array. (c) 3D bar graph displaying the real-time relative current variation in (b). (d) Photographs of the MTP pressure sensor array with 3D-printed numbers “1”, “9”, “0”, and “4” positioned on top. (e) Color contrast mapping and (f) 3D bar graph to show the real-time relative current variation in (d).

$$\mathrm{SNR} = 10 \times \log \frac{V_{\mathrm{rmsl}}}{V_{\mathrm{rmsn}}}$$

where V_{rmsl} and V_{rmsn} are the root-mean-square values of the ECG signal without and with noise. The SNR value (30.6 dB) of the ECG signals measured by the MXene/tissue paper electrodes is much higher than 21.4 dB from the commercial Ag/AgCl gel electrodes. With two electrodes on the forearm and the MTP pressure sensor on the wrist (Figure 4g), the ECG and pulse signals are continuously recorded (Figure 4h). After obtaining the pulse transit time (PTT) between the R-peak in the ECG and the epidermal pulse maximum of each cardiac cycle, the real-time SBP and DBP can be extracted using the PTT mehthod[51] (Figure 4i). In brief, the PTT method indicates that the mean blood pressure (P) is correlated with the elastic modulus (E) of the blood artery by Hughes equation:[52] $E = E_0 e^{\alpha P}$, where $\alpha = 0.017$ mmHg^{-1}. The PTT is inversely proportional to the pulse wave velocity (PWV) for a short elastic vessel, which is described by the Moens-Korteweg equation:[53]

$$\mathrm{PWV} = \frac{\mathrm{distance}}{\mathrm{PTT}} = \sqrt{\frac{Eh}{\rho 2r}}$$

where h and r are the thickness and radius of the blood vessel and ρ is the blood density. By assuming negligibly small changes in the vessel thickness and radius, the mean blood pressure is connected with PTT via a logarithmic relationship: PTT as $P = k\ \ln(\mathrm{PTT}) + b$. As a result, the SBP and DBP can be obtained as a function of PTT as

$$\mathrm{DBP} = \frac{\mathrm{SBP}_0}{3} + \frac{2\mathrm{DBP}_0}{3} + A\ \ln\left(\frac{\mathrm{PTT}_0}{\mathrm{PTT}}\right) - \frac{(\mathrm{SBP}_0 - \mathrm{DBP}_0)}{3}\frac{\mathrm{PTT}_0{}^2}{\mathrm{PTT}^2}$$

$$\mathrm{SBP} = \mathrm{DBP} + (\mathrm{SBP}_0 - \mathrm{DBP}_0)\frac{\mathrm{PTT}_0{}^2}{\mathrm{PTT}^2}$$

where SBP_0 and DBP_0 are determined by a commercial sphygmomanometer from a one-time calibration, A is a subject-dependent coefficient (can be estimated for the

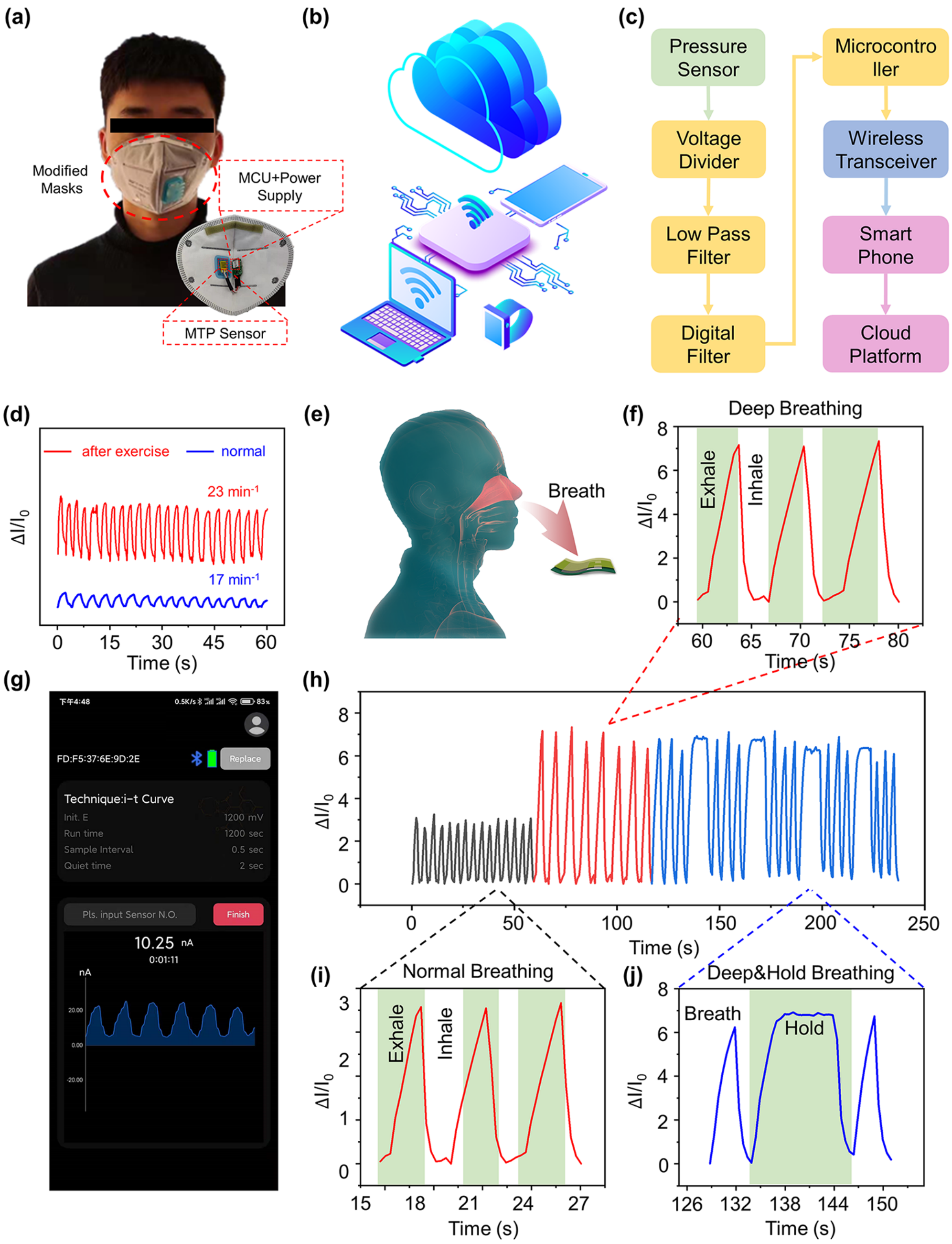

FD:F5:37:6E:9D:2E

Technique:i–t Curve
Init. E 1200 mV
Run time 1200 sec
Sample Interval 0.5 sec
Quiet time 2 sec

Pls. input Sensor N.O.

10.25 nA
0:01:11

Figure 6. Smart mask that integrates the flexible pressure sensor with power supply and wireless transmission modules for respiration monitoring and opioid overdose detection. (a) Photograph to show the human subject wearing the smart mask with each module labeled in the inset. (b) Schematic illustrations and (c) block diagram of the entire remote monitoring platform. (d) Relative current variation of the sensor induced by respiration before (blue) and after (red) exercise, with the testing schematic for human exhaled air detection shown in (e). The normal breath signal on the remote real-time monitoring interface is shown in (g). (h) Breath signals from three different breathing patterns: normal (black) with a zoom-in view in (i), deep (red) with a zoom-in view in (f), and deep and holding breath (blue) with a zoom-in view in (j). Holding the breath simulates respiratory arrest.

population[52]), and PTT_0 is the initial PTT of the first recorded cycle. While there is no significant change in the DBP after exercise, the SBP after exercise is generally higher than that before exercise (Figure 4i). Notably, the difference in the DBP and SBP between those measured by our soft sensors and a commercial sphygmomanometer is less than 5% (Figure 4j), which features the highly reliable blood pressure measurement from the noninvasive soft sensors.

The individual MTP pressure sensors can also be configured into an array layout for detecting spatial pressure distribution. As an example, the pressure sensor array with 4 × 4 units on a single interdigital electrode matrix (Figure 5a and Figure S18a) can identify the position and pressure magnitude induced by two weights (i.e., 5 and 10 g) placed on two different pixels of the matrix (Figure 5b,c). Furthermore, the representative 3D-printed numbers (e.g., "1", "9", "0", and "4") can also be distinguished by the pressure array as shown in the color contrast mapping and a 3D bar graph (Figure 5d–f). The object with an irregular shape such as a key can be accurately detected by the sensor array as well (Figure S18b,c). While the

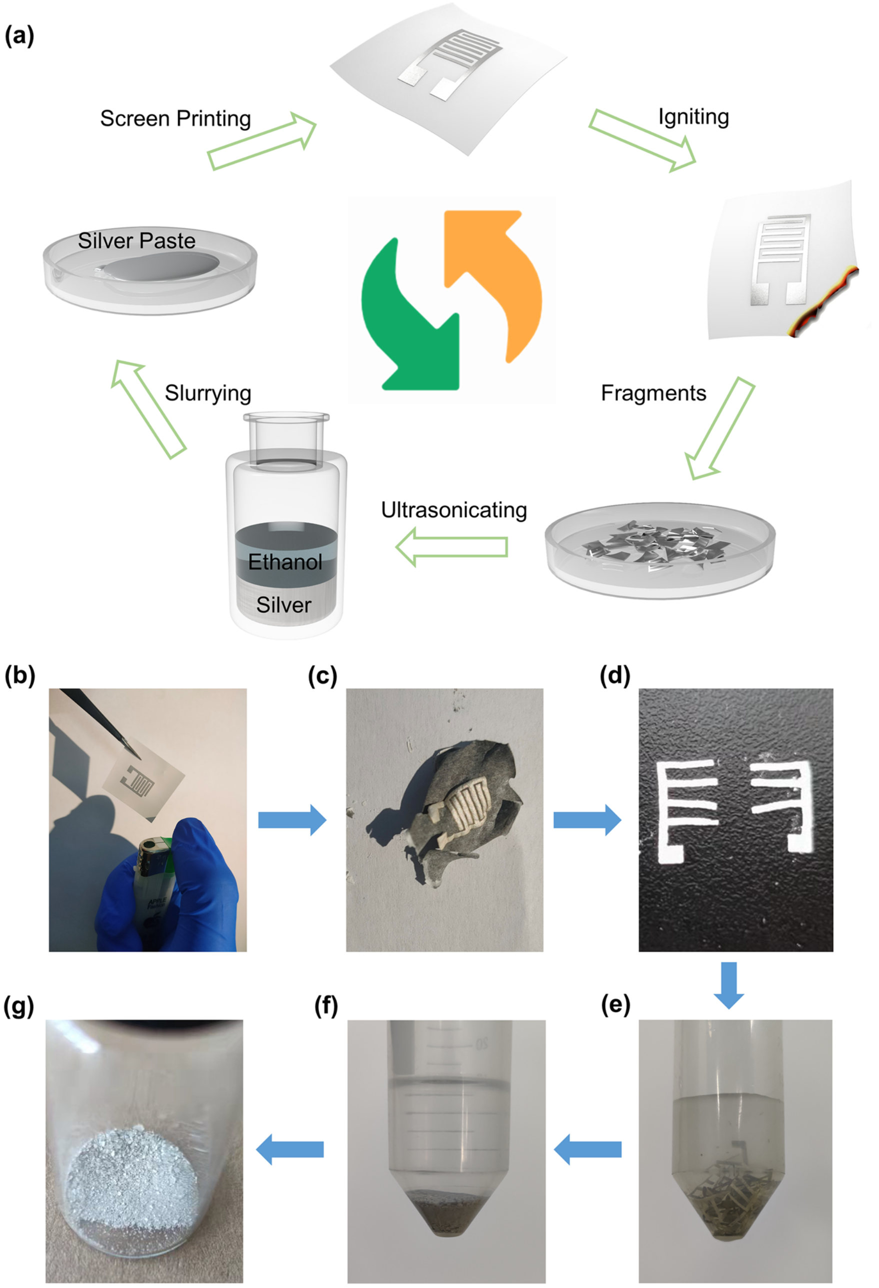

Figure 7. Recycling of Ag interdigital electrode in the all-paper-based MTP pressure sensor. (a) Schematic of the recycling procedure for the Ag interdigital electrodes. Images of the printing paper with the silver interdigital electrode (b) before and (c) after burning. After (d) separating and (e) collecting the fragmented silver interdigital electrode with ethanol, (f) sonication and (g) drying of the solution yields the silver powder.

pressure sensor array is connected to the back of the human hand, it can map the spatial pressure distribution as well as the toy bear placed on the top (Figure S19), opening up opportunities in the electronic skin, human−machine interfaces, and intelligent prostheses.

2.5. Remote Respiration Monitoring System. Because there exists an urgent and unmet need for real-time detection of an opioid overdose[54] especially for illicit opioid use,[55] it is highly desirable to develop a remote respiration monitoring system for early self-identification of the opioid overdose. The remote respiration monitoring system that integrates the flexible MTP pressure sensor with signal processing and wireless communication module on a face mask (Figure 6a) is developed to capture the opioid-induced respiratory depression.[56] The MTP pressure sensor placed in the middle of the breathing valve gives a higher relative current change compared with those placed on the left or right side (Figure S20) due to a stronger breathing airflow. As shown in the flowchart (Figure 6b,c), the remote respiratory monitoring system first converts the resistance change of the MTP pressure sensor to a voltage value through a voltage divider, removes the noise by a low pass filter, and then digitizes the signal using a 16-bit $\delta{-}\sigma$ modulator. The digitized signals wirelessly transmitted via a Bluetooth module can visualize the signal on the smartphone (the schematic diagram of the circuit shown in Figure S21). As the breathing flow changes the resistance of the MTP pressure sensor (Figure 6e), the real-time respiratory pattern from a healthy human subject (24 years old, male) before and after intense exercise can be recorded (Figure 6d) and wirelessly transmitted to smartphones (Figure 6g). From the exhalation and inhalation cycles, the respiration rate can be calculated to show an increase in the rate from 17 to 23 min^{-1} after exercise (Figure 6d). The measurements are within 5% of those detected by a medical device (Mindray, PM-7000) (Figure S22), indicating highly reliable respiratory rate recording from our remote respiration monitoring system. Besides, the larger amplitude of the signal waveform also indicates the deep respiratory activities after exercise. On the basis of this observation, the remote monitoring system is applied to detect normal breathing, deep breathing, and holding the breath for 12 s after three times of deep breathing for simulated respiratory arrest (Figure 6f−j). It is worth noting that the relative current remains constant when the human subject holds his breath. The current system to detect respiratory abnormalities can be applied for opioid overdose, pulmonary fibrosis, and other cardiopulmonary diseases.

2.6. All-Paper-Based MTP Pressure Sensor and Its Recycling Process. Replacing the PI tape with weighing paper yields an all-paper-based MTP pressure sensor (Figure S23a), which still exhibits high sensitivity (344.0 or 15.4 kPa^{-1} in the ranges 0.5−30 or 30−100 kPa) in the same broad detection range 0.5−100 kPa (Figure S23b−d). Though the sensitivity of the all-paper-based MTP pressure sensor is smaller than that with the thin PI encapsulation, the sensing performance is still superior to most previously reported ones (Table S1). More importantly, the all-paper-based MTP sensor allows for recycling of the silver interdigital electrode (Figure 7a). In brief, burning of the used sensor for 20 s turns the paper to ash with the silver interdigital electrode remaining intact. After separating and collecting the fragmented silver interdigital electrode with ethanol, a cell crusher with ultrasound at a power of 300 W was then used for 60 min. Placing the resulting solution in a vacuum drying oven obtained the silver powder for reuse.

3. CONCLUSIONS

In summary, we have explored the design, characterization, and demonstration of a MTP pressure sensor based on the highly porous 3D structure of MXene/tissue paper. The MTP pressure sensor shows an ultrahigh sensitivity of 509.5 kPa^{-1}, a low limit (1 Pa) and broad range (0.5 to 100 kPa) of detection, and outstanding stability over 10 000 loading/unloading cycles. The flexible MTP sensor with ultrahigh sensitivity over a broad pressure range and fast response/recovery is suitable to monitor varying physiological signals (e.g., pulse, phonation, and respiration) and motion states (e.g., standing, walking, and jumping). The concurrent measurement of pulse and ECG signals also allows for the continuous measurements of the SBP and DBP. By configuring individual MTP pressure sensors into an array layout, the resulting smart artificial E-skin can detect spatial pressure distribution for human−machine interfaces and intelligent prostheses. Integrating the MTP pressure sensor with signal processing and wireless communication modules on a face mask conveniently yields a smart face mask as a remote respiration monitoring system. The wirelessly detected respiratory abnormalities on the smartphone provide early self-identification of the opioid overdose. The design of the integrated wireless remote respiration monitoring system can also be adapted and applied for pulmonary fibrosis and other cardiopulmonary diseases. Furthermore, we have fabricated an all-paper-based MTP pressure sensor by replacing the thin PI encapsulation with a weighing paper so that the incineration allows for recycling of the sliver interdigital electrodes to avoid electronic waste.

4. EXPERIMENTAL SECTION

Materials. The printing papers (Deli, Ningbo, China) and PI tape (Kapton) were used as substrate and encapsulation layer of the MTP pressure sensor, respectively. The tissue paper (Vinda, Jiangmen, China) was used to fabricate the MXene/tissue paper. The silver paste was purchased from Ausbond. The copper foils (T = 0.05 mm) were used to connect the MTP pressure sensor to the digital source meter.

Synthesis of MXene Power and Dispersion. MXene ($Ti_3C_2T_x$) was synthesized by selective etching of Al from MAX (Ti_3AlC_2) as in ref 57. Briefly, 0.8 g of LiF was first added to 10 mL of HCl (9 M), followed by stirring for 5 min at room temperature. Next, 0.5 g of Ti_3AlC_2 powder was gradually added into the above mixture over the course of >5 min, followed by the reaction at 35 °C over continuous stirring for 24 h. The reaction mixture was then washed with deionized (DI) water several times by centrifugation at 3500 rpm (until reaching near 7 in the pH of the supernatant). Separating the black slurry from the gray solid (unetched Ti_3AlC_2) yielded $Ti_3C_2T_x$ powder. After adding 0.1 g of $Ti_3C_2T_x$ powder into 100 mL of DI water with sonication for several minutes at 200 W, centrifuging at 3000 rpm for 20 min removed the unexfoliated aggregates and $Ti_3C_2T_x$ MXene dispersion was stored as obtained. The concentration of the MXene dispersion was prepared in the range from 0.5 to 1.0 mg/mL (0.6 mg/mL chosen unless otherwise specified).

Preparation of the MXene/Tissue Paper (MTP) and MTP Pressure Sensor. The tissue paper was cut into a rectangular shape of 10 × 10 mm^2 and immersed in MXene dispersion for 10 s. Annealing at 40 °C in a vacuum drying chamber for 40 min fully evaporated the water to yield the MTP. Next, the printing paper with interdigital electrodes was prepared by screen printing (200 mesh) and drying of silver paste at room temperature. Sandwiching the MTP between a PI encapsulation layer and a printing paper with an interdigitated electrode resulted in the MTP pressure sensor. The connection between the electrodes and the data acquisition system was made by two copper foils via silver paste.

Characterization. SEM and TEM images were recorded by a field emission SEM (JEOL, JSM 7100F) and Tecnai G2 F20 HRTEM, respectively. A D8 Advance (Bruker) X-ray diffractometer and ESCALAB 250 photoelectron spectrometer (Thermo Fisher Scientific) were used to measure XRD patterns and XPS, respectively. The external pressure was loaded by a universal materials testing machine (JSV-H1000). The piezoresistive properties of the MTP pressure sensor were measured by a Keithley 2400 source meter at 1 V. The pressure distribution from the 4 × 4 pressure sensor array was detected in real-time by a microcontroller (Arduino Mega 2560) connected to a computer using a custom-built MATLAB (Math Works) program.

■ ASSOCIATED CONTENT

Supporting Information

The Supporting Information is available free of charge at https://pubs.acs.org/doi/10.1021/acsami.1c22001.

Movie of MTP pressure sensor (MP4)

Figures of cross-section morphology of the MTP pressure sensor, dimension and photograph of the printing paper with the interdigitated electrodes, photographs of the tissue paper and MTP, equivalent circuit diagram of the MTP pressure sensor, XPS measurments of MXene powder, SEM image of tissue paper, sheet resistance of the MTP sheet prepared by different concentrations of the MXene dispersion, dependence of the sensitivity on the sheet resistance of MXene/tissue paper, sensing performance of the MTP pressure sensor with varying encapsulation thicknesses and different MXene/tissue paper layers, average sensor performance measured from five samples, repeatability test of the MTP sensor over 10 000 cycles for pressures of 10 and 30 kPa, response/recovery rates of the MTP pressure sensor, bending deformation test of the MTP pressure sensor, sensor response induced by three different motion states with the sensor below the insole, single-pulse waveforms before and after exercise, photograph of MXene/tissue paper electrodes for ECG measurement, ECG signals measured with commercial Ag/AgCl gel electrodes and the MXene/tissue paper electrodes, electrodes of the sensor array and the color contrast mapping of a key, image of the sensor array attached to the back of the human hand, breathe signals from three different pressure sensor locations of the mask, schematic of the remote respiration monitoring system, comparisons of the respiratory rates measured by the remote respiration monitoring system and a medical device, and electromechanical properties of the flexible all-paper-based MTP pressure sensor and its performance comparison with other flexible pressure sensors and table of comparison of sensitivity and detection limit of the MTP pressure sensor with other flexible pressure sensors (PDF)

AUTHOR INFORMATION

Corresponding Authors

Li Yang – *State Key Laboratory of Reliability and Intelligence of Electrical Equipment, Department of Electrical Engineering, Hebei University of Technology, Tianjin 300130, China;* orcid.org/0000-0001-6798-3177; Email: yangli5781@126.com

Huanyu Cheng – *Department of Engineering Science and Mechanics, The Pennsylvania State University, University Park, Pennsylvania 16802, United States;* orcid.org/0000-0001-6075-4208; Email: huanyu.cheng@psu.edu

Authors

Hongli Wang – *Department of Mechanical Engineering, Hebei University of Technology, Tianjin 300130, China*

Wenjing Yuan – *Tianjin Key Laboratory of Materials Laminating Fabrication and Interface Control Technology, Department of Materials Science & Engineering, Hebei University of Technology, Tianjin 300130, China*

Yuhang Li – *Institute of Solid Mechanics, Beihang University (BUAA), Beijing 100191, China*

Peng Gao – *Department of Electronic Information, Hebei University of Technology, Tianjin 300130, China*

Naveen Tiwari – *Department of Engineering Science and Mechanics, The Pennsylvania State University, University Park, Pennsylvania 16802, United States;* orcid.org/0000-0002-4252-3235

Xue Chen – *Department of Mechanical Engineering, Hebei University of Technology, Tianjin 300130, China*

Zihan Wang – *Department of Mechanical Engineering, Hebei University of Technology, Tianjin 300130, China*

Guangyu Niu – *Department of Architecture and Art, Hebei University of Technology, Tianjin 300130, China*

Complete contact information is available at: https://pubs.acs.org/10.1021/acsami.1c22001

Notes

The authors declare no competing financial interest.

ACKNOWLEDGMENTS

This work was supported by the National Natural Science Foundation of China (51705126 and 61871173), and the Key Research and Development Project of Hebei Province (20271701D). H.C. acknowledges the supports provided by NSF (Grant No. ECCS-1933072), NIH (Award Nos. R61HL154215 and R21EB030140), and Penn State University.

REFERENCES

(1) Zhang, H.; Niu, W.; Zhang, S. Extremely Stretchable and Self-Healable Electrical Skin with Mechanical Adaptability, an Ultrawide Linear Response Range, and Excellent Temperature Tolerance. *ACS Appl. Mater. Interfaces* **2019**, *11* (27), 24639–24647.

(2) Wang, Q.; Jian, M.; Wang, C.; Zhang, Y. Carbonized Silk Nanofiber Membrane for Transparent and Sensitive Electronic Skin. *Adv. Funct. Mater.* **2017**, *27* (9), 1605657.

(3) Zhang, L.; He, J.; Liao, Y.; Zeng, X.; Qiu, N.; Liang, Y.; Xiao, P.; Chen, T. A Self-Protective, Reproducible Textile Sensor with High Performance Towards Human-Machine Interactions. *J. Mater. Chem. A* **2019**, *7* (46), 26631–26640.

(4) Qi, J.; Yang, P.; Waraich, A.; Deng, Z.; Zhao, Y.; Yang, Y. Examining Sensor-Based Physical Activity Recognition and Monitoring for Healthcare Using Internet of Things: A Systematic Review. *J. Biomed. Inf.* **2018**, *87*, 138–153.

(5) Yan, C.; Deng, W.; Jin, L.; Yang, T.; Wang, Z.; Chu, X.; Su, H.; Chen, J.; Yang, W. Epidermis-Inspired Ultrathin 3D Cellular Sensor Array for Self-Powered Biomedical Monitoring. *ACS Appl. Mater. Interfaces* **2018**, *10* (48), 41070–41075.

(6) Huang, Y.; Wang, Z.; Zhou, H.; Guo, X.; Zhang, Y.; Wang, Y.; Liu, P.; Liu, C.; Ma, Y.; Zhang, Y. Highly Sensitive Pressure Sensor Based on Structurally Modified Tissue Paper for Human Physiological Activity Monitoring. *J. Appl. Polym. Sci.* **2020**, *137*, 48973.

(7) Yang, L.; Yi, N.; Zhu, J.; Cheng, Z.; Yin, X.; Zhang, X.; Zhu, H.; Cheng, H. Novel Gas Sensing Platform Based on A Stretchable Laser-Induced Graphene Pattern with Self-Heating Capabilities. *J. Mater. Chem. A* **2020**, *8*, 6487–6500.

(8) Yi, N.; Cheng, Z.; Li, H.; Yang, L.; Zhu, J.; Zheng, X.; Chen, Y.; Liu, Z.; Zhu, H.; Cheng, H. Stretchable, Ultrasensitive, and Low-Temperature NO_2 Sensors Based on MoS_2@rGO Nanocomposites. *Mater. Today Physics* **2020**, *15*, 100265.

(9) Mousavi, S.; Howard, D.; Zhang, F.; Leng, J.; Wang, C. H. Direct 3D Printing of Highly Anisotropic, Flexible, Constriction-Resistive Sensors for Multidirectional Proprioception in Soft Robots. *ACS Appl. Mater. Interfaces* **2020**, *12* (13), 15631–15643.

(10) Zhou, L. Y.; Gao, Q.; Zhan, J. F.; Xie, C. Q.; Fu, J. Z.; He, Y. Three-Dimensional Printed Wearable Sensors with Liquid Metals for Detecting the Pose of Snakelike Soft Robots. *ACS Appl. Mater. Interfaces* **2018**, *10* (27), 23208–23217.

(11) Li, W.; Jin, X.; Zheng, Y.; Chang, X.; Wang, W.; Lin, T.; Zheng, F.; Onyilagha, O.; Zhu, Z. A Porous and Air Gap Elastomeric Dielectric Layer for Wearable Capacitive Pressure Sensor with High Sensitivity and A Wide Detection Range. *J. Mater. Chem. C* **2020**, *8* (33), 11468–11476.

(12) Yang, J.; Luo, S.; Zhou, X.; Li, J.; Fu, J.; Yang, W.; Wei, D. Flexible, Tunable, and Ultrasensitive Capacitive Pressure Sensor with Microconformal Graphene Electrodes. *ACS Appl. Mater. Interfaces* **2019**, *11* (16), 14997–15006.

(13) Chamankar, N.; Khajavi, R.; Yousefi, A. A.; Rashidi, A.; Golestanifard, F. A Flexible Piezoelectric Pressure Sensor Based on PVDF Nanocomposite Fibers Doped with PZT Particles for Energy Harvesting Applications. *Ceram. Int.* **2020**, *46* (12), 19669–19681.

(14) Hosseini, E. S.; Manjakkal, L.; Shakthivel, D.; Dahiya, R. Glycine-Chitosan-Based Flexible Biodegradable Piezoelectric Pressure Sensor. *ACS Appl. Mater. Interfaces* **2020**, *12* (8), 9008–9016.

(15) Jiang, J.; Tu, S.; Fu, R.; Li, J.; Hu, F.; Yan, B.; Gu, Y.; Chen, S. Flexible Piezoelectric Pressure Tactile Sensor Based on Electrospun $BaTiO_3$/Poly(vinylidene fluoride) Nanocomposite Membrane. *ACS Appl. Mater. Interfaces* **2020**, *12* (30), 33989−33998.
(16) Meng, L.; Xu, Q.; Dan, L.; Wang, X. Single-Walled Carbon Nanotube Based Triboelectric Flexible Touch Sensors. *J. Electron. Mater.* **2019**, *48* (11), 7411−7416.
(17) Wang, H. L.; Kuang, S. Y.; Li, H. Y.; Wang, Z. L.; Zhu, G. Large-Area Integrated Triboelectric Sensor Array for Wireless Static and Dynamic Pressure Detection and Mapping. *Small* **2020**, *16* (2), No. 1906352.
(18) Guo, Y.; Zhong, M.; Fang, Z.; Wan, P.; Yu, G. A Wearable Transient Pressure Sensor Made with MXene Nanosheets for Sensitive Broad-Range Human-Machine Interfacing. *Nano Lett.* **2019**, *19* (2), 1143−1150.
(19) Chen, S.; Song, Y.; Xu, F. Flexible and Highly Sensitive Resistive Pressure Sensor Based on Carbonized Crepe Paper with Corrugated Structure. *ACS Appl. Mater. Interfaces* **2018**, *10* (40), 34646−34654.
(20) Wu, Q.; Qiao, Y.; Guo, R.; Naveed, S.; Hirtz, T.; Li, X.; Fu, Y.; Wei, Y.; Deng, G.; Yang, Y.; Wu, X.; Ren, T. L. Triode-Mimicking Graphene Pressure Sensor with Positive Resistance Variation for Physiology and Motion Monitoring. *ACS Nano* **2020**, *14* (8), 10104−10114.
(21) Han, Z.; Li, H.; Xiao, J.; Song, H.; Li, B.; Cai, S.; Chen, Y.; Ma, Y.; Feng, X. Ultralow-Cost, Highly Sensitive, and Flexible Pressure Sensors Based on Carbon Black and Airlaid Paper for Wearable Electronics. *ACS Appl. Mater. Interfaces* **2019**, *11* (36), 33370−33379.
(22) Li, T.; Chen, L.; Yang, X.; Chen, X.; Zhang, Z.; Zhao, T.; Li, X.; Zhang, J. A Flexible Pressure Sensor based on an MXene-Textile Network Structure. *J. Mater. Chem. C* **2019**, *7* (4), 1022−1027.
(23) Bi, L.; Yang, Z.; Chen, L.; Wu, Z.; Ye, C. Compressible AgNWs/$Ti_3C_2T_x$ MXene Aerogel-Based Highly Sensitive Piezoresistive Pressure Sensor as Versatile Electronic Skins. *J. Mater. Chem. A* **2020**, *8* (38), 20030−20036.
(24) Zhu, Y.; Cai, H.; Ding, H.; Pan, N.; Wang, X. Fabrication of Low-Cost and Highly Sensitive Graphene-Based Pressure Sensors by Direct Laser Scribing Polydimethylsiloxane. *ACS Appl. Mater. Interfaces* **2019**, *11* (6), 6195−6200.
(25) Cheng, Y.; Ma, Y.; Li, L.; Zhu, M.; Yue, Y.; Liu, W.; Wang, L.; Jia, S.; Li, C.; Qi, T.; Wang, J.; Gao, Y. Bioinspired Microspines for a High-Performance Spray $Ti_3C_2T_x$ MXene-Based Piezoresistive Sensor. *ACS Nano* **2020**, *14* (2), 2145−2155.
(26) Luo, C.; Liu, N.; Zhang, H.; Liu, W.; Yue, Y.; Wang, S.; Rao, J.; Yang, C.; Su, J.; Jiang, X.; Gao, Y. A New Approach for Ultrahigh-Performance Piezoresistive Sensor Based on Wrinkled PPy Film with Electrospun PVA Nanowires as Spacer. *Nano Energy* **2017**, *41*, 527−534.
(27) Tao, L.-Q.; Zhang, K.-N.; Tian, H.; Liu, Y.; Wang, D.-Y.; Chen, Y.-Q.; Yang, Y.; Ren, T.-L. Graphene-Paper Pressure Sensor for Detecting Human Motions. *ACS Nano* **2017**, *11* (9), 8790−8795.
(28) Yang, T.; Mativetsky, J. M. Paper-Based Mechanical Sensors Enabled by Folding and Stacking. *ACS Appl. Mater. Interfaces* **2019**, *11* (29), 26339−26345.
(29) Duan, Z.; Jiang, Y.; Huang, Q.; Wang, S.; Zhao, Q.; Zhang, Y.; Liu, B.; Yuan, Z.; Wang, Y.; Tai, H. Facilely Constructed Two-Sided Microstructure Interfaces between Electrodes and Cellulose Paper Active Layer: Eco-Friendly, Low-Cost and High-Performance Piezoresistive Sensor. *Cellulose* **2021**, *28* (10), 6389−6402.
(30) Li, F.; Qin, Q.; Zhou, Y.; Wu, Y.; Xue, W.; Gao, S.; Shang, J.; Liu, Y.; Li, R.-W. Recyclable Liquid Metal-Based Circuit on Paper. *Adv. Mater. Technologies* **2018**, *3*, 1800131.
(31) Zhu, B.; Niu, Z.; Wang, H.; Leow, W. R.; Wang, H.; Li, Y.; Zheng, L.; Wei, J.; Huo, F.; Chen, X. Microstructured Graphene Arrays for Highly Sensitive Flexible Tactile Sensors. *Small* **2014**, *10* (18), 3625−3631.
(32) Park, J.; Kim, J.; Hong, J.; Lee, H.; Lee, Y.; Cho, S.; Kim, S.-W.; Kim, J. J.; Kim, S. Y.; Ko, H. Tailoring Force Sensitivity and Selectivity by Microstructure Engineering of Multidirectional Electronic Skins. *NPG Asia Mater.* **2018**, *10* (4), 163−176.
(33) Ji, B.; Zhou, Q.; Wu, J.; Gao, Y.; Wen, W.; Zhou, B. Synergistic Optimization toward the Sensitivity and Linearity of Flexible Pressure Sensor via Double Conductive Layer and Porous Microdome Array. *ACS Appl. Mater. Interfaces* **2020**, *12* (27), 31021−31035.
(34) Ji, B.; Mao, Y.; Zhou, Q.; Zhou, J.; Chen, G.; Gao, Y.; Tian, Y.; Wen, W.; Zhou, B. Facile Preparation of Hybrid Structure Based on Mesodome and Micropillar Arrays as Flexible Electronic Skin with Tunable Sensitivity and Detection Range. *ACS Appl. Mater. Interfaces* **2019**, *11* (31), 28060−28071.
(35) Wang, Z.; Zhang, L.; Liu, J.; Jiang, H.; Li, C. Flexible Hemispheric Microarrays of Highly Pressure-Sensitive Sensors Based on Breath Figure Method. *Nanoscale* **2018**, *10* (22), 10691−10698.
(36) Liu, W.; Liu, N.; Yue, Y.; Rao, J.; Luo, C.; Zhang, H.; Yang, C.; Su, J.; Liu, Z.; Gao, Y. A Flexible and Highly Sensitive Pressure Sensor Based on Elastic Carbon Foam. *J. Mater. Chem. C* **2018**, *6* (6), 1451−1458.
(37) Gao, L.; Zhu, C.; Li, L.; Zhang, C.; Liu, J.; Yu, H.-D.; Huang, W. All Paper-Based Flexible and Wearable Piezoresistive Pressure Sensor. *ACS Appl. Mater. Interfaces* **2019**, *11* (28), 25034−25042.
(38) Gong, S.; Schwalb, W.; Wang, Y.; Chen, Y.; Tang, Y.; Si, J.; Shirinzadeh, B.; Cheng, W. A Wearable and Highly Sensitive Pressure Sensor with Ultrathin Gold Nanowires. *Nat. Commun.* **2014**, *5* (1), 3132.
(39) Zhu, B.; Ling, Y.; Yap, L. W.; Yang, M.; Lin, F.; Gong, S.; Wang, Y.; An, T.; Zhao, Y.; Cheng, W. Hierarchically Structured Vertical Gold Nanowire Array-Based Wearable Pressure Sensors for Wireless Health Monitoring. *ACS Appl. Mater. Interfaces* **2019**, *11* (32), 29014−29021.
(40) Zhan, Z.; Lin, R.; Tran, V. T.; An, J.; Wei, Y.; Du, H.; Tran, T.; Lu, W. Paper/Carbon Nanotube-Based Wearable Pressure Sensor for Physiological Signal Acquisition and Soft Robotic Skin. *ACS Appl. Mater. Interfaces* **2017**, *9* (43), 37921−37928.
(41) Long, Y.; He, P.; Xu, R.; Hayasaka, T.; Shao, Z.; Zhong, J.; Lin, L. Molybdenum-Carbide-Graphene Composites for Paper-Based Strain and Acoustic Pressure Sensors. *Carbon* **2020**, *157*, 594−601.
(42) Xia, K.; Wang, C.; Jian, M.; Wang, Q.; Zhang, Y. CVD Growth of Fingerprint-Like Patterned 3D Graphene Film for an Ultrasensitive Pressure Sensor. *Nano Res.* **2018**, *11* (2), 1124−1134.
(43) Yue, Y.; Liu, N.; Liu, W.; Li, M.; Ma, Y.; Luo, C.; Wang, S.; Rao, J.; Hu, X.; Su, J.; Zhang, Z.; Huang, Q.; Gao, Y. 3D Hybrid Porous MXene-Sponge Network and Its Application in Piezoresistive Sensor. *Nano Energy* **2018**, *50*, 79−87.
(44) Gao, Y.; Yan, C.; Huang, H.; Yang, T.; Tian, G.; Xiong, D.; Chen, N.; Chu, X.; Zhong, S.; Deng, W.; Fang, Y.; Yang, W. Microchannel-Confined MXene Based Flexible Piezoresistive Multifunctional Micro-Force Sensor. *Adv. Funct. Mater.* **2020**, *30* (11), 1909603.
(45) Hu, Y.; Zhuo, H.; Luo, Q.; Wu, Y.; Wen, R.; Chen, Z.; Liu, L.; Zhong, L.; Peng, X.; Sun, R. Biomass Polymer-Assisted Fabrication of Aerogels From MXenes with Ultrahigh Compression Elasticity and Pressure Sensitivity. *J. Mater. Chem. A* **2019**, *7* (17), 10273−10281.
(46) Chao, M.; He, L.; Gong, M.; Li, N.; Li, X.; Peng, L.; Shi, F.; Zhang, L.; Wan, P. Breathable $Ti_3C_2T_x$ MXene/Protein Nanocomposites for Ultrasensitive Medical Pressure Sensor with Degradability in Solvents. *ACS Nano* **2021**, *15* (6), 9746−9758.
(47) Cheng, H.; Wang, S. Mechanics of Interfacial Delamination in Epidermal Electronics Systems. *ASME. J. Appl. Mech* **2014**, *81* (4), 044501.
(48) Li, M.; Liang, J.; Wang, X.; Zhang, M. Ultra-Sensitive Flexible Pressure Sensor Based on Microstructured Electrode. *Sensors* **2020**, *20*, 371.
(49) Blacher, J.; Asmar, R.; Djane, S.; London, G. M.; Safar, M. E. Aortic Pulse Wave Velocity as A Marker of Cardiovascular Risk in Hypertensive Patients. *Hypertension* **1999**, *33*, 1111−1117.
(50) Zahed, M. A.; Das, P. S.; Maharjan, P.; Barman, S. C.; Sharifuzzaman, M.; Yoon, S. H.; Park, J. Y. Flexible and Robust Dry Electrodes Based on Electroconductive Polymer Spray-coated 3D

Porous Graphene for Long-Term Electrocardiogram Signal Monitoring System. *Carbon* **2020**, *165*, 26−36.

(51) McCarthy, B. M.; O'Flynn, B.; Mathewson, A. An Investigation of Pulse Transit Time as a Non-Invasive Blood Pressure Measurement Method. *J. Phys.: Conf. Ser.* **2011**, *307*, 012060.

(52) Hughes, D. J.; Babbs, C. F.; Geddes, L. A.; Bourland, J. D. Measurements of Young's Modulus of Elasticity of the Canine Aorta with Ultrasound. *Ultrasonic Imaging* **1979**, *1* (4), 356−367.

(53) Peter, J.; Czuwala. McDonald's Blood Flow in Arteries: Theoretical, Experimental and Clinical Principles. *Echocardiography* **1991**, *8* (3), 405−406.

(54) Mishra, R. K.; Goud, K. Y.; Li, Z.; Moonla, C.; Mohamed, M. A.; Tehrani, F.; Teymourian, H.; Wang, J. Continuous Opioid Monitoring Along with Nerve Agents on a Wearable Microneedle Sensor Array. *J. Am. Chem. Soc.* **2020**, *142* (13), 5991−5995.

(55) Romero, R. A.; Young, S. D. Adolescents and Opioid-Related Outcomes Amidst the COVID-19 Pandemic. *J. Addict. Dis.* **2021**, No. 11, 1−8.

(56) Cheng, S.-M.; Chan, J. J. I.; Tan, C. W.; Lu, E.; Sultana, R.; Sng, B. L. Use of Wireless Respiratory Rate Sensor Monitoring During Opioid Patient-Controlled Analgesia After Gynaecological Surgery: A Prospective Cohort Study. *Indian J. Anaesth.* **2021**, *65* (2), 146−152.

(57) Kim, S. J.; Koh, H.-J.; Ren, C. E.; Kwon, O.; Maleski, K.; Cho, S.-Y.; Anasori, B.; Kim, C.-K.; Choi, Y.-K.; Kim, J.; Gogotsi, Y.; Jung, H.-T. Metallic $Ti_3C_2T_x$ MXene Gas Sensors with Ultrahigh Signal-to-Noise Ratio. *ACS Nano* **2018**, *12* (2), 986−993.

■ NOTE ADDED AFTER ASAP PUBLICATION

This paper originally published ASAP on December 13, 2021. Minor changes were made througout the paper and a new version was reposted on December 13, 2021.